FEASIBILITY STUDY OF A SYNTHESIS PROCEDURE FOR ARRAY FEEDS TO IMPROVE RADIATION PERFORMANCE OF LARGE DISTORTED REFLECTOR ANTENNAS

SEMIANNUAL STATUS REPORT

submitted to
NASA Langley Research Center
for
Grant No. NAG-1-859

by

W.L. Stutzman
K. Takamizawa
P. Werntz
J. LaPean
R. Barts
B. Shen

Virginia Polytechnic Institute and State University
Bradley Department of Electrical Engineering
Blacksburg, Virginia 24061-0111

August 1991

TABLE OF CONTENTS

1. INTRODUCTION

Virginia Tech is involved in a number of activities with NASA Langley related to large aperture radiometric antenna systems. These efforts are summarized in Table 1-1. This semi-annual report is primarily directed toward the grant first listed in Table 1-1; however, some results for all activities are reported here as well.

Table 1-2 lists the major reflector antenna research areas together with the students performing the work. Table 1-3 details specific tasks in each of the intensive work areas. This report is organized into sections reflective of the work areas as listed in Table 1-3.

Table 1-1

REFLECTOR ANTENNA RESEARCH AT VIRGINIA TECH

1. "Feasibility Study of a Synthesis Procedure for Array Feeds to Improve Radiation Performance of Large Distorted Reflector Antennas"

   GAs: Ko Takamizawa, Jim LaPean, Paul Werntz
   Project: NASA Grant NAG-1-859; VT 4-26132
   Term: 02/25/88 - 12/31/91

2. "Design of Array Feeds for Large Reflector Antennas"

   GA: Mike Barts
   Project: NASA Graduate Student Researchers Program; NGT-50413; VT 4-26204
   Term: 08/16/89 - 08/15/92

PERSONNEL ACTIVE IN REFLECTORS BUT NOT SUPPORTED BY NASA

3. Bing Shen, Ph.D. student
   Dissertation topic: Reflector Antenna Synthesis with Application to Scanning Systems with Spherical or Shaped Main Reflectors

4. Derrick Dunn, M.S. student
   GEM Fellowship
   New student

Table 1-2

REFLECTOR ANTENNA RESEARCH ACTIVITIES AT VIRGINIA TECH

I. Technology Development
- 1.1. Operation and testing of full commercial reflector code (GRASP7) - Takamizawa
- 1.2. Multiple reflector cylindrical antenna code (MRAPCA) - Takamizawa
- 1.3. Documentation of analysis techniques for reflector computations - Takamizawa
- 1.4. Development of synthesis codes
- 1.5. Canonical cases - Takamizawa and Dunn

II. Wide Scanning Antenna Systems
- 2.1. Documentation of wide scanning antenna principles - Werntz
- 2.2. Type 2 tri reflector antenna design - Werntz
- 2.3. Type 6 dual reflector design - LaPean
- 2.4. Support of Type 6 hardware model - LaPean
- 2.5. Spherical reflector antenna design - Shen
- 2.6. Other concepts
  - Dual parabolic reflector - Takamizawa
  - Cylindrical reflector family
  - Toroidal reflector family
  - Hybrid concepts

III. Reflector System Optimization - Takamizawa
- 3.1 Comparison of optimization techniques
- 3.2 Application of optimization using PO
- 3.3 Error functional definition

IV. Arrays for Large Radiometric Antennas - Barts
- 4.1. Analysis techniques in lossy radiometric systems using arrays.
- 4.2. Feed array architectures for radiometers
- 4.3. Feed component technology readiness evaluation
- 4.4. Calibration issues
- 4.5. Beam efficiency studies

Table 1-3
RESEARCH PLAN FOR FOCUS AREAS

II. Wide Scanning Antenna Systems

- 2.1 Documentation of wide scanning antenna principles - Werntz
- 2.2 Type 2 tri reflector antenna design - Werntz
  - 2.2.1 Cassegrain configurations
    - 2.2.1.1 Rotation of tertiary
    - 2.2.1.2 Rotation and translation of tertiary
    - 2.2.1.3 Shaped subreflector
    - 2.2.1.4 Conclusion of Cassegrain configuration
  - 2.2.2 Gregorian configurations
    - 2.2.2.1 Feed-above subreflector results
    - 2.2.2.2 Feed-under subreflector results
    - 2.2.2.3 Conclusion of Gregorian results
- 2.3 Type 6 dual reflector antenna design - LaPean
  - 2.3.1 Moving subreflector 2D - complete
  - 2.3.2 Moving subreflector 3D
  - 2.3.3 Array feed support
  - 2.3.4 Dual shaped Type 6 system
- 2.4 Support of Type 6 hardware model - LaPean
  - 2.4.1 Movable subreflector to scan 1 degree
  - 2.4.2 Type 2 class feed assembly
    - 2.4.2.1 0° scan angle
    - 2.4.2.2 5° scan angle
- 2.5 Spherical reflector antenna design - Shen
  - 2.5.1

III. Reflector System

- 3.1 Comparison of optimization technique
  - 3.1.1 Geometrical averaging
  - 3.1.2 Geometrical optics analysis
  - 3.1.3 Physical optics analysis
- 3.2 Application of optimization using PO
  - 3.2.1 Type 2 tri reflector
  - 3.2.2 Type 6 dual reflector
- 3.3 Error functional definition
  - 3.3.1 RMS phase error
  - 3.3.2 Aberration components in aperture fields
  - 3.3.3 Zernike polynomial expansion of amplitude and phase
  - 3.3.4 Maximizing beam efficiency

IV. Radiometric Arrays

- 4.1 Development of noise modeling methodology for arrays
- 4.2 Development of noise scene modeling for arrays
- 4.3 Evaluation of candidate array architecture noise performance
- 4.4 Development of candidate radiometer calibration techniques

2. TECHNOLOGY DEVELOPMENT

This area supports the investigation areas, primarily in the form of computer code development for analysis of reflector antenna radiation patterns. Here we report on the two main codes in active use.

2.1 Status of Codes

Two analysis programs are used for verification and evaluation of synthesis techniques: Multiple Reflector Antenna Program for Cylindrical Antenna (MRAPCA) and General Reflector Antenna Systems Program (GRASP). The program MRAPCA was developed at Virginia Tech to analyze two dimensional multiple cylindrical reflector antennas with arbitrary configurations. The patterns are computed using near-field physical optics/aperture integration (NF-PO/AI) and far-field physical optics/aperture integration (FF-PO/AI) on all reflectors. The program is very close to the final form. A report on the EM analysis and the numerical techniques and the users guide to the program is being written.

GRASP is a commercially available code to evaluate radiation patterns of three dimensional single or dual reflectors. The program uses a combination of the physical optics/aperture integration (PO/AI) and the geometrical theory of diffraction (GTD) to compute the patterns. The code also has a capability to analyze N-reflector systems by N-1 runs of the program. Initially, GRASP program was installed on IBM 3090 mainframe at Virginia Tech. During this reporting period, the program was also installed on Intel 30486 and Intel 30386 based IBM PC/AT compatible computers at Virginia Tech. The 486 machine also has NDP-FORTRAN.

2.2 Canonical Cases

In order to evaluate performance and accuracy of the results from the GRASP program, studies of several canonical configurations were conducted. Table 2.2-1 lists canonical cases analyzed and the other cases that are under investigation.

2.3 Surface Interpolation

Preliminary results on the canonical reference case 20 in Table 2.2-1 show that the surface interpolation routine for non-uniformly distributed surface data points using the routine IBIRAN is not acceptable at high frequencies. In the course of this study, it was noted that the method of defining reflector surfaces has large impact on the results of both in analysis and synthesis of reflector antennas. This problem has been discussed by many authors without a definite conclusion. [1-4] Rahmat-Samii states that there is no universal interpolation technique which applies efficiently and accurately to all cases. [5] A surface

Table 2.2-1 Reflector Canonical Cases

Canonical Reference No.	Test Number	Person Res	Description
1	TEST9	KT	Prime focus, axisymmetric D = 100λ, F/D = 0.5 CSC feed pattern giving uniform aperture illumination
2	TEST10	KT	Prime focus, axisymmetric D = 100λ, F/D = 0.5 Feed pattern giving parabolic aperture taper (p = 1, C = 0)
3	TEST11	KT	Prime focus, axisymmetric D = 100λ, F/D = 0.5 Feed pattern giving parabolic aperture taper (p = 2, C = 0)
4	TEST12	KT	Prime focus, axisymmetric D = 100λ, F/D = 0.5 Feed pattern giving parabolic aperture taper (p = 1, C=-10 dB)
5	TEST7	KT	Prime focus, axisymmetric D = 100λ, F/D = 1.0, dipole feed
6	TEST8	KT	Prime focus, axisymmetric D = 100λ, F/D = 0.5, dipole feed
7	TEST15	KT	Offset prime focus D = 100λ, F/D = 0.5 CSC feed pattern giving uniform aperture illumination
8	TEST16	KT	Offset prime focus D = 100λ, F/D = 0.5 Feed pattern giving parabolic aperture taper (p = 1, C = 0)
9	TEST17	KT	Offset prime focus D = 100λ, F/D = 0.5 Feed pattern giving parabolic aperture taper (p = 2, C = 0)
10	TEST18	KT	Offset prime focus D = 100λ, F/D = 0.5 Feed pattern giving parabolic aperture taper (p = 1, C=-10 dB)

11	TEST13	KT	Offset prime focus D = 100λ, F/D = 1.0, dipole feed
12	TEST14	KT	Offset prime focus D = 100λ, F/D = 0.5, dipole feed
13			Offset prime focus [R-11]
14			Offset prime focus [R-15]
15			Axisymmetric Cassegrain
16			Offset Cassegrain TICRA Test Case No. 2 D = 38.93λ, F/D = 0.736
17			Offset Cassegrain Rahmat-Samii from Lo & Lee Book
18			[L-62] Offset Cassegrain
19			Integration convergence test Near field, Hyperbola, F = 10 GHz to 60 GHz
20			IBIRAN test
21			Beam efficiency test
22			[A-30] D=3m, F=3m, h=0.45m, f=4 GHz Sq. feed horn, Diag. horn, CP feed, Multimode
23			[R-78] Beam squint, D = 20λ, F =8λ
24		KT	[R-] Focal plane fields
25			[R-83] TE_{10} WG feed
26	TEST19	KT	Rahmat-Samii potato chip reflector
27	TDRS1~4	KT	Harris TDRS
28			Prodelin antenna
29			[R-85] Rappaport, elliptical main reflector
30			[L-63] Bi-parabolic main reflector

interpolation technique suitable to our application is under investigation.

2.4 References

[1] Y. Rahmat-Samii, V. Galido-Israel, "A novel global surface interpolation for reflector antenna application," *1981 National Radio Science Meeting*, Boulder, Colorado, Jan., 1982.

[2] F.L. Teixeira, C.G. Rego, J.R. Bergmann and F.J.V. Hasselmann, "Application of pseudo-splines for global surface interpolation in shaped reflector synthesis," *Proceedings ICAP 1991*, York, pp. 9-12, April, 1991.

[3] A.K. Brown, R. Atimebdi, "Implementation of numerical surface fitting techniques in reflector antenna design and manufacture," *Proceedings ICAP 1991*, York, pp. 452-455, April, 1991.

[4] L.A. Baker, "The Clam Shell Problem - Interpolation of shaped reflectors and other smooth surfaces," *IEEE Trans. Antennas Propagat.*, Vol. AP-36, pp. 1560-1565, Nov. 1988.

[5] Y. Rahmat-Samii, "Effects of deterministic surface distortion on reflector antenna performance," *Antennes De Télécommunication*," Vol. 40, No. 7-8, 1985.

3. PERFORMANCE ANALYSIS OF A NOVEL TRI-REFLECTOR ANTENNA CONFIGURATION (TYPE 2)

3.1 Introduction

The reflector antenna configurations discussed in this section are derived from a reflector configuration originally proposed by Foldes [1]. The purpose of this reflector configuration is to allow for beam scanning with a minimum of reflector motion and no feed motion. The elimination of feed motion is particularly important. This is because the feed will most likely consist of several phased arrays in order to allow for both the correction of scan induced phase errors (and phase errors due to intrinsic reflector surface errors) and cover the required bandwidth of 20-60 GHz. Therefore, because of the large mass of such a feed, reflector designs which eliminate feed motion are very attractive. A second reason why feed motion should be avoided is because the flexible cables necessary to accommodate motion reduce reliability and may cause calibration problems for radiometric applications.

The original reflector purposed by Foldes (the Foldes Type 2 reflector antenna [2]) consists of a parabolic main reflector and an elliptic subreflector in a Cassegrain configuration and a shaped tertiary reflector. The elliptic subreflector has one focus point at the center of the main reflector and the other focus point at

the center of the tertiary. This creates a conjugate relationship between these two points. Ideally, any ray incident on the center of the main reflector, regardless of incidence angle, will be reflected to the conjugate point at the center of the tertiary. This insures that the center of the tertiary will remain stationary for all scan directions. Therefore, to first order, the main beam of this reflector configuration can be scanned by a rotation of the tertiary reflector (which is relatively small) about the center conjugate point.

A cross sectional view of the original Foldes type 2 reflector system is shown in Fig. 3-1. The computer program used to generate this reflector configuration is the Three Reflector Antenna Synthesis Code (TRAS). TRAS is a geometrical optics (ray tracing) synthesis code which can be used to obtain a shaped tertiary reflector for any main reflector, subreflector, feed position and scan angle combination such that there are no aperture plane phase errors (in a geometrical optics sense). The dimensions of this reflector diameter is 28 m and the focal length of the main reflector is 55.9 m (F/D = 2). The configuration shown in Fig. 3-1 is designed to scan ± 2.5° and requires a subreflector diameter of 10.5 m to prevent spillover throughout this scan range. Three tertiary positions corresponding to scan directions of 2.5°, 0° and -2.5° are shown in Fig. 3-1 along with the ray paths of the rays striking the top, center and bottom of the main reflector from each of the three scan directions. In order to provide undistorted scanning (correct for scan induced phase errors) and provide full main reflector illumination, the tertiary must be allows to vary in both size and shape over the scan range. In this case the tertiary diameter varies from approximately 35 m to 6.7 m, the smallest tertiary size corresponding to the -2.5° scan direction and the largest size corresponding to the 2.5° scan direction. Despite a slight change in tertiary shape and a drastic change in tertiary size, the tertiary does rotate about the central conjugate point as is shown in the detail of tertiary motion in Fig. 3-2.

The Foldes Type 2 reflector configuration has several disadvantages [3]. First, a symmetric tertiary illumination leads to a unsymmetric main reflector illumination necessitating a feed capable of precise pattern control. Second, the tertiary diameter has a wide variation in size over the scan range and the diameter is unacceptably large for the positive scan directions. Because the tertiary diameter would have to be limited to a reasonable size, the result is gain loss due to tertiary spillover for positive scan directions. Finally, because of the angle with which the subreflector intercepts the rays reflected off of the main reflector, a large subreflector is needed.

A configuration which has been shown to overcome the disadvantage of the Foldes Type 2 reflector system is the Gregorian tri-reflector system [3]. The Gregorian tri-reflector is based on the same principle of using an elliptic subreflector to create a

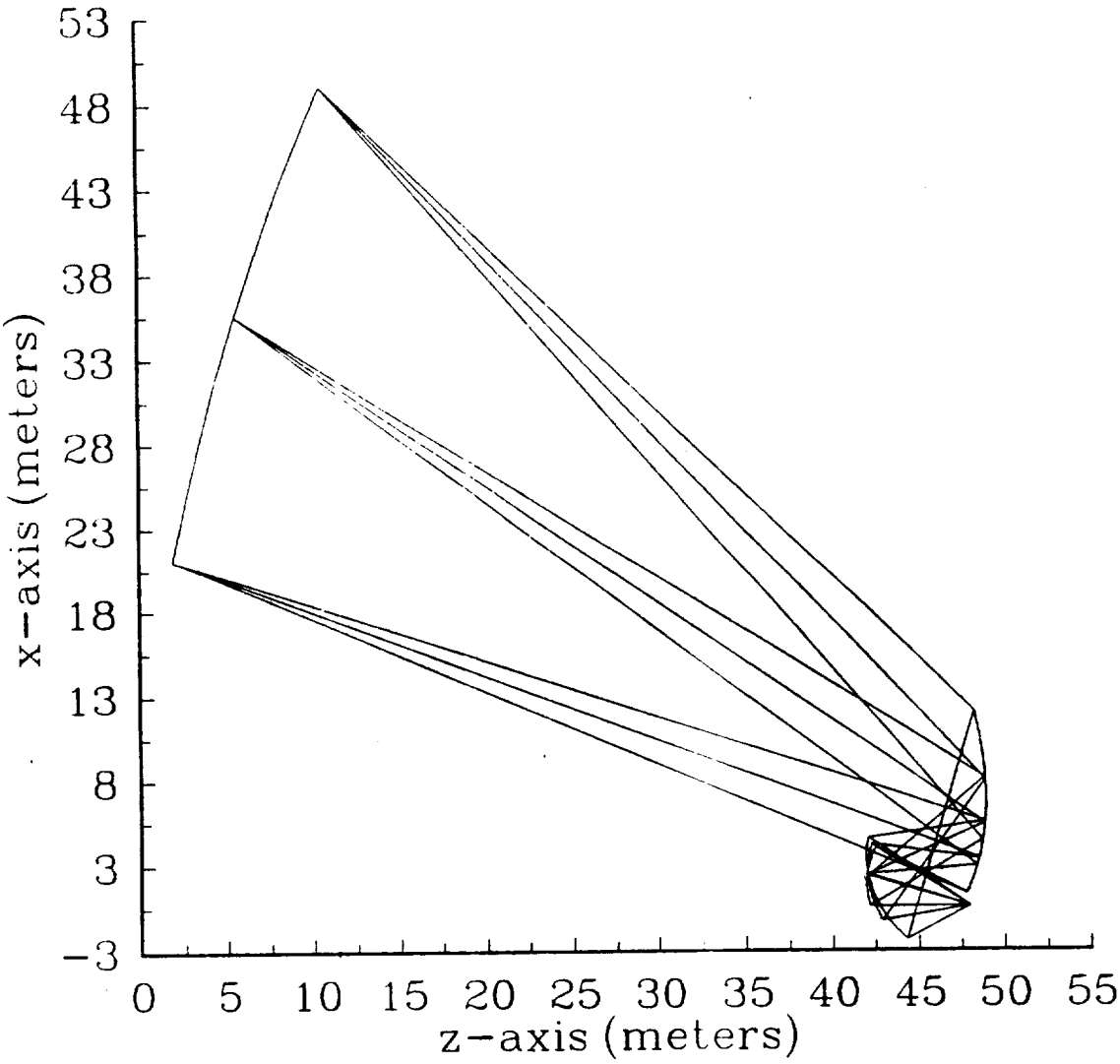

Figure 3-1. Original Foldes Type 2 reflector configuration consisting of a parabolic main reflector an elliptical subreflector in a Cassegrain configuration and a shaped tertiary reflector. Shown is a system designed to scan ±2.5°.

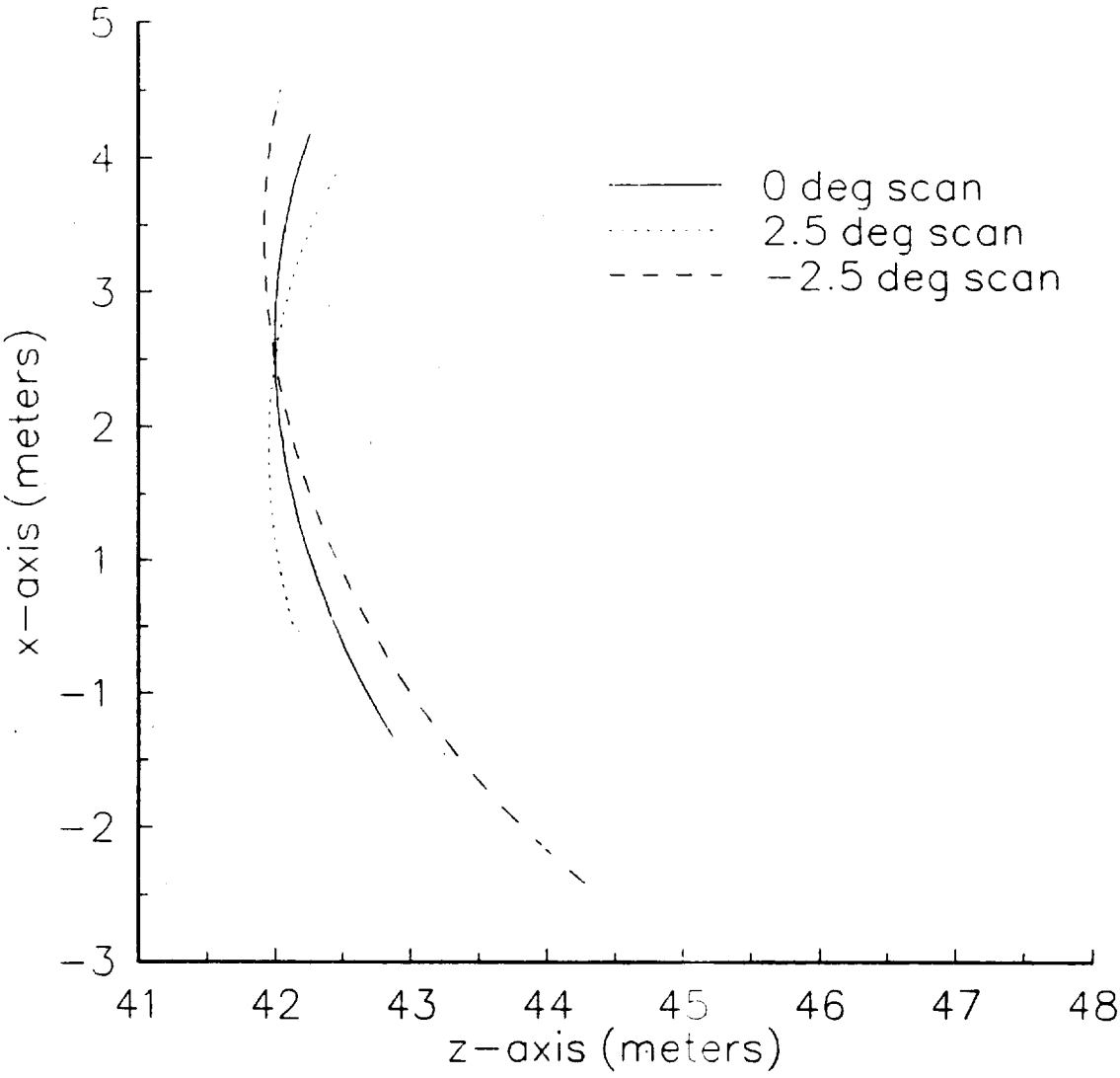

Figure 3-2. **Tertiary positions at the scan limits of the Foldes Type 2 reflector antenna.**

conjugate relationship between the point at the center of the main reflector and the center of the tertiary. The difference between the Gregorian tri-reflector and the Foldes Type 2 reflector is that in the Gregorian system, the subreflector is placed beyond the focal point of the main reflector. An example Gregorian tri-reflector is shown in Fig. 3-3. This reflector system has a main reflector diameter of 25 m with a focal length of 30 m. The bottom of the main reflector is offset by 8 m from the axis of parabolic symmetry. The configuration shown in Fig. 3-3 is designed to scan ±5° (compared to the Foldes Type 2 reflector system in Fig. 3-1 which is only capable of scanning ±2.5°) and requires a subreflector diameter of 10.89 m to prevent spillover over this scan range. The largest tertiary size needed is 5.5 m corresponding to the +5° direction of scan and the smallest tertiary size needed is 4.13 m corresponding to the -5° scan direction.

As with the Foldes Type 2 reflector system, simply rotating a fixed shape tertiary reflector to scan the resultant beam does not correct for all of the scan induced phase errors. In the following, preliminary results from a continuing study on the effects of feed position and tertiary motion on the magnitude of scan induced phase errors and tertiary size are presented.

3.2 Scan Characteristics Study

In this section, TRAS is used as part of an algorithm to assess the relationship between feed location and scan characteristics for the Gregorian tri-reflector shown in Fig. 3-3. In this study, it is assumed that the scan mechanism is limited to only a rotation and/or translation of a fixed shape tertiary reflector. In all cases the fixed shape tertiary corresponds to the tertiary designed to provide error free scanning in the boresight direction (the unscanned case). This study is based on two dimensional structures only (cylindrical reflector surfaces) and a two dimensional version of TRAS called TRAS2D is used.

In order to evaluate the scan characteristics, TRAS2D is used to generate shaped tertiaries for the unscanned case and for scanned cases in the 5° and -5° directions. An optimization routing is then used to best fit the tertiary corresponding to the unscanned case to the tertiaries corresponding to the two scan directions. The RMS error between the surfaces provides a figure of merit which is related to the scan induced phase error. The actual relationship between the RMS surface error and the resultant phase error has yet to be determined.

With reference to Fig. 3-4, the error between two tertiary surfaces at any point is defined as being the difference between z-displacement, Δz_i, for a given x position, x_i with the reference reflector positioned such that the center passes through the origin with the surface normal pointing in the positive z direction. This

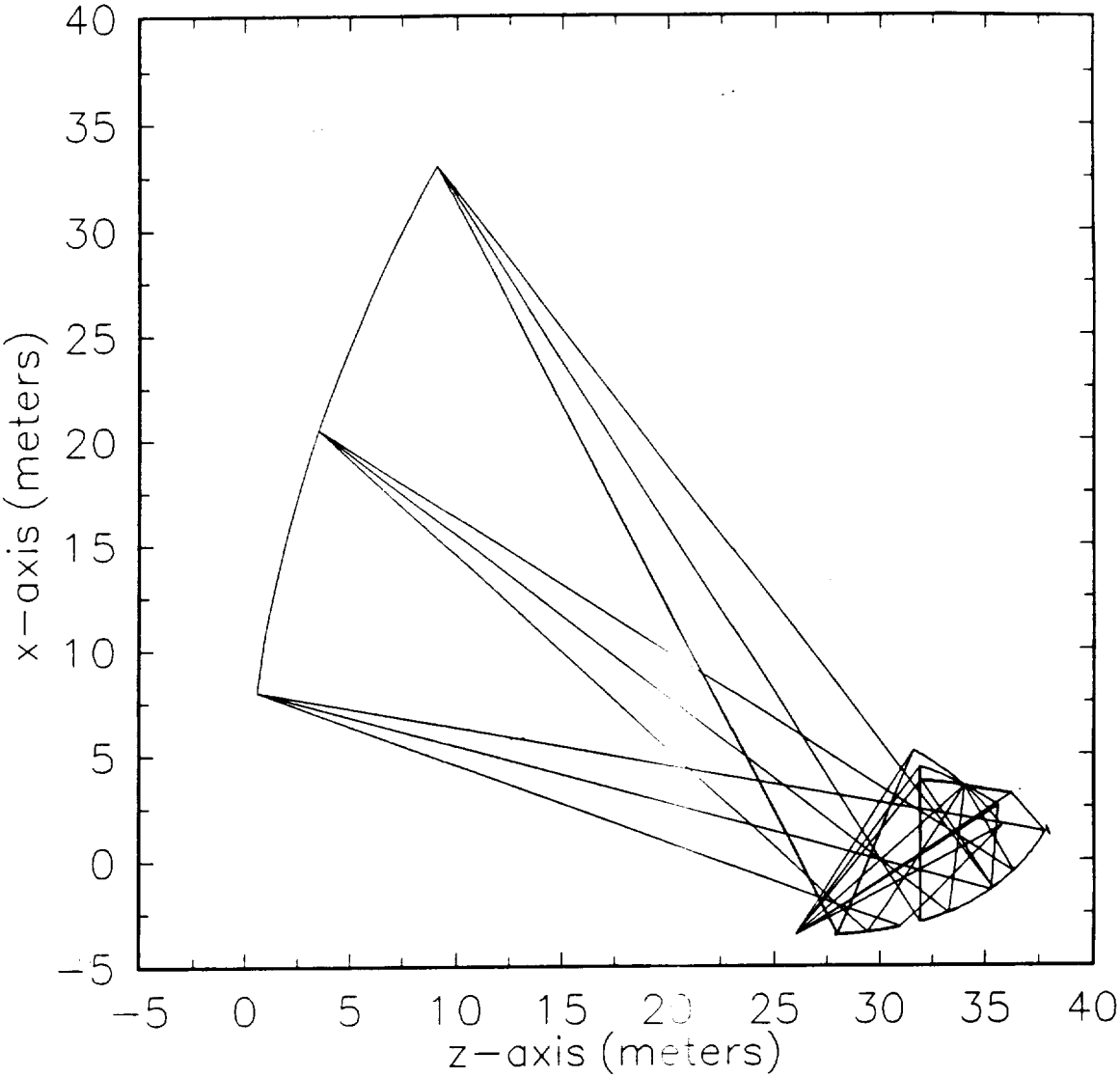

Figure 3-3. Gregorian tri-reflector antenna consisting of a parabolic main reflector, an elliptic subreflector in a Gregorian configuration and a shaped tertiary reflector. Shown is a system designed to scan ±5°.

measurement is made for 20 samples spaced Δx apart over the extent of the smaller reflector. The RMS error is then defined as

$$\varepsilon_{RMS} = \sqrt{\left(\sum_{i=1}^{N} \Delta z_i^2\right) \div N} \qquad (3\text{-}1)$$

Where N = 20 samples spaced Δx apart.

In order to assess the effect of feed location on the RMS surface error for 5° and -5° scan directions, the feed was moved along the elliptical arc of the subreflector from a z position of z = 26 m (shown in Fig. 3-3) to a z position of z = 38 m (which places the feed just above the top edge of the subreflector). Figure 3-5 shows a plot of the RMS surface error versus feed position for the +5° scan case. Five lines are drawn on this plot. The top line shows the surface error of the unscanned tertiary movement is restricted to only a rotation about its center. The next line down shows the surface error if a linear translation in any direction of not more than 0.25 m is allows along with the rotation. Likewise the next two lines down show the surface error if the tertiary is allowed a maximum translation of 0.5 m and 0.75 m respectively. Finally, the bottom line corresponds to the surface error if unrestricted tertiary translation is allowed. Figure 3-6 is for the -5° scan direction. At the point of this writing, no explanation for the jagged appearance of some of the curves has been found. As these are preliminary findings, numerical error has not been ruled out; however, no errors in the optimization code used to best fit the reflector surfaces has been found to date.

An interesting feature in Fig. 3-5 is the existence of a distinct feed location on the subreflector, at z ≈ 36.5 m, where surface error is minimized if tertiary motion is limited to only rotation (the top line in Fig. 3-5). It is suspected that a similar error minimum exists for the -5° scan direction; however, its location is off of the right side of the plot. While there is an optimum feed location in terms of scan error for the 5° scan direction, it is not the best location in terms of tertiary dimension. This is shown in Fig. 3-7 which presents a plot of tertiary diameter versus feed location for the 5°, 0° and -5° scan directions. According to Fig. 3-7, the tertiary size for the 5° scan direction increases rapidly beyond a feed position of z ≈ 33.5 m. The reflector configuration which results from placing the feed on the subreflector at z = 36.5 m is shown in Fig. 3-8. The tertiary size for this configuration varies from approximately 3.0 m to 6.33 m, with the largest corresponding to the 5° scan direction. Because it causes ray blockage, the large tertiary corresponding to the 5° scan direction would have to be truncated in this configuration resulting in tertiary spillover and reduced

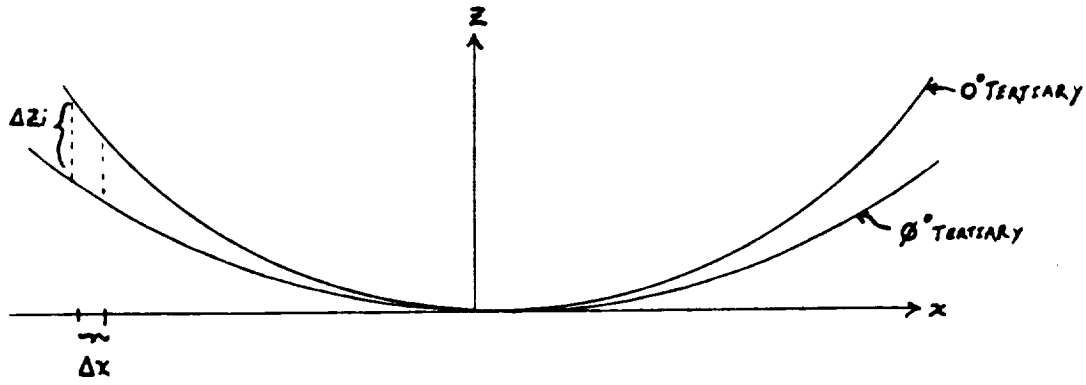

Figure 3-4. The scan error between the tertiary designed to scan 0° and the tertiary designed to scan angle ϕ. The error, ΔZ_i is evaluated at points i.

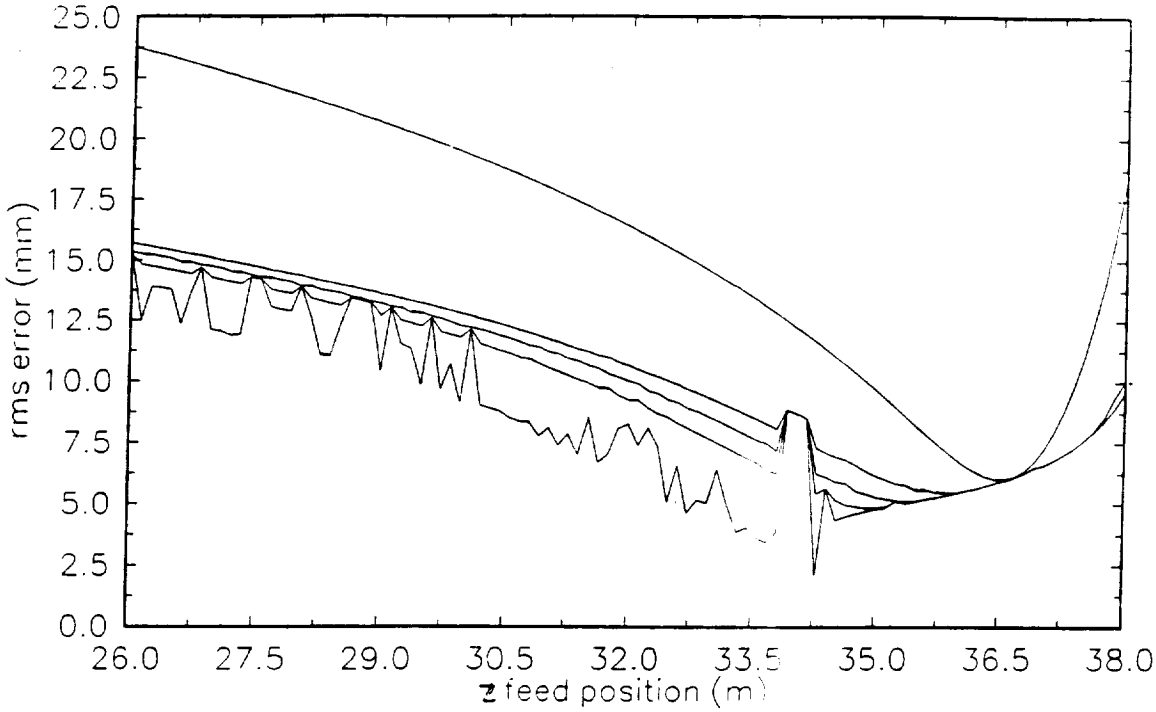

Figure 3.5. RMS surface error versus z coordinate of the feed position along the subreflector for the 5° scan direction. The top curve corresponds to motion limited to only rotation. From top to bottom, the next 3 curves represent the RMS error if the maximum translation is restricted to be less than 0.25 m, 0.5 m and 0.75 m. The bottom curve corresponds to the case of unlimited translation.

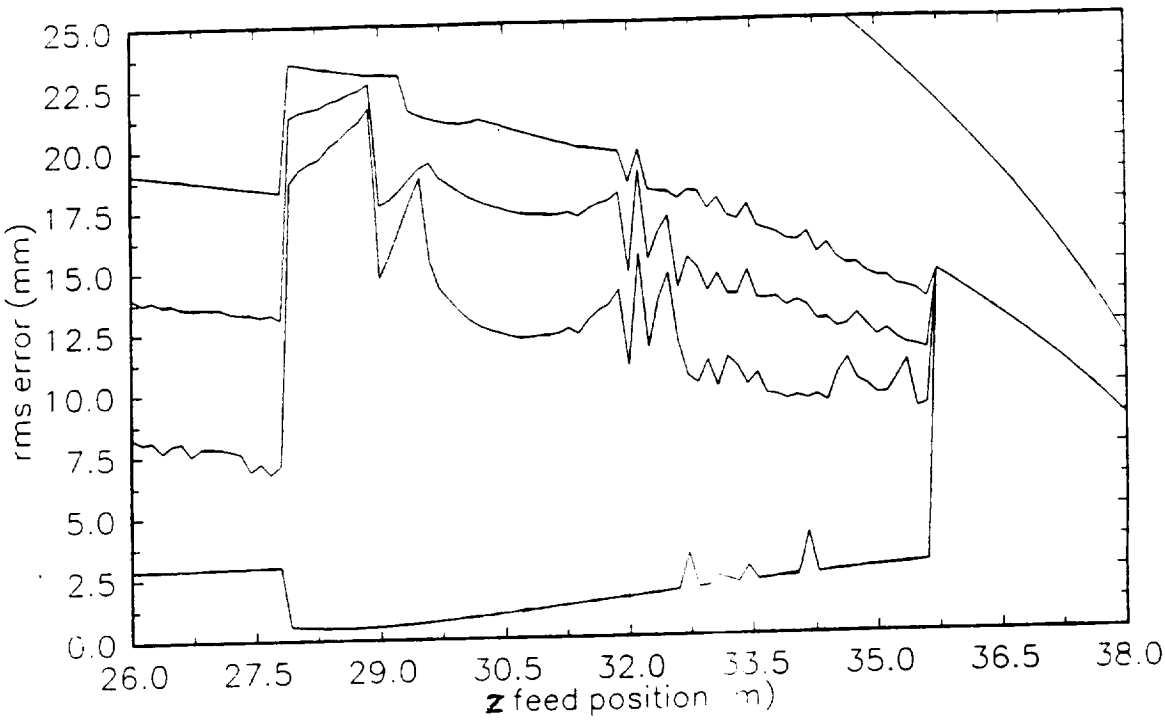

Figure 3-6. RMS surface error versus z coordinate of the feed position along the subreflector from the -5° scan direction. The top curve corresponds to motion limited to only rotation. From top to bottom, the next 3 curves represent the RMS error if the maximum translation is restricted to be less than 0.25 m, 0.5 m and 0.75 m. The bottom curve corresponds to the case of unlimited translation.

gain on reception. According to Fig. 3-7, the best feed location in terms of minimizing both tertiary size and tertiary size variation over the scan range is at z ≈ 26.0 m. The reflector configuration resulting from placing the feed in this location is shown in Fig. 3-3. However, according to Figs. 3-5 and 3-6, this is a bad location in terms of scan induced phase errors.

Another interesting feature of Figs. 3-5 and 3-6 is the large amount of error improvement, except in the vicinity of the optimum feed location in Fig. 3-5, obtained by allowing a translation of only 0.25 m. However, the unnatural appearance of some of the curves, particularly for the -5° scan direction prevents any further speculation until the suspect features can be verified.

3.3 Conclusions

(1) Figure 3-5 indicates the location of an optimum feed position in terms of minimizing the change in tertiary shape for the 5° scan direction. This position is on the subreflector at z = 36.5.

(2) Figure 3-7 indicates that the feed position that minimizes scan induced phase errors does not correspond to the best feed location of the reflector configuration physical dimensions.

(3) Considerable improvement in scan induced phase errors can be obtained by allowing even a small amount of tertiary translation.

3.4 Recommendations for Future Work

(1) Verify the optimization code used to best fit the tertiary corresponding to different scan directions.

(2) Attempt to find physical explanations for the features of the curves shown in Figs. 3-5 and 3-6. Particularly for the location of the error minimum in Fig. 3-5.

(3) Attempt to find a reflector configuration which has a feed location for minimum tertiary shape change which corresponds more closely to the feed location which gives the most desirable physical characteristics.

(4) Extend the present analysis to three dimensions.

3.5 References

[1] P. Foldes, Foldes Inc., 1131 Radnor Hill Road, Wayne, PA 19087.

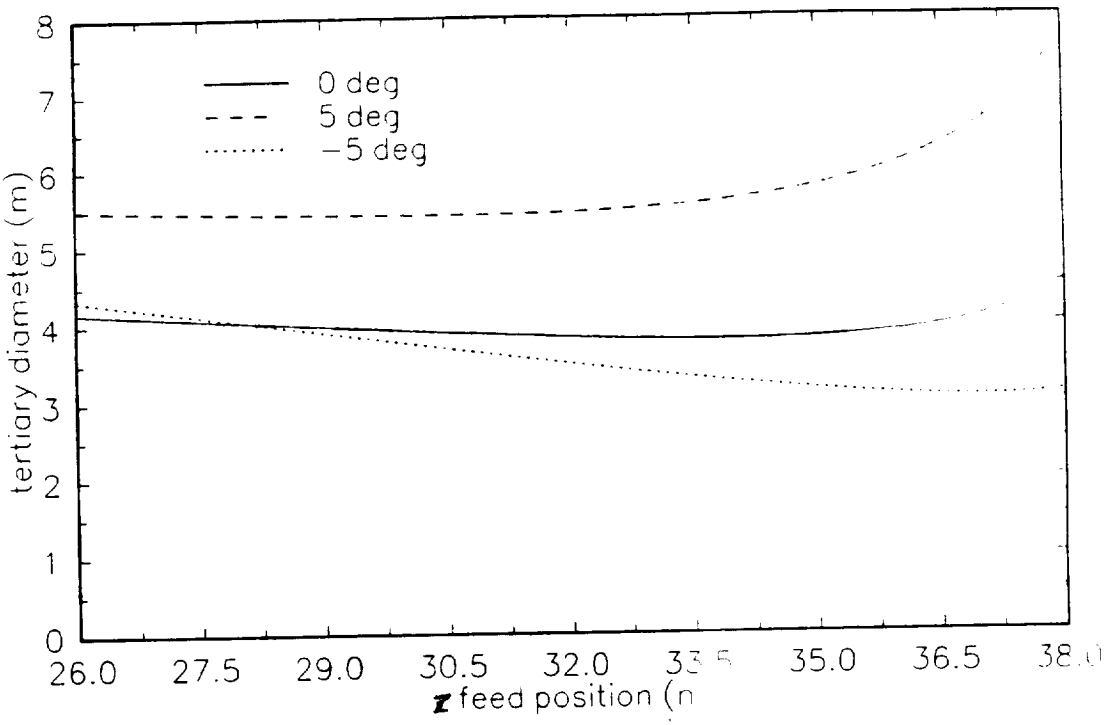

Figure 3-7. **Tertiary diameter versus z coordinate of the feed position for 5°, 0° and -5° scan directions.**

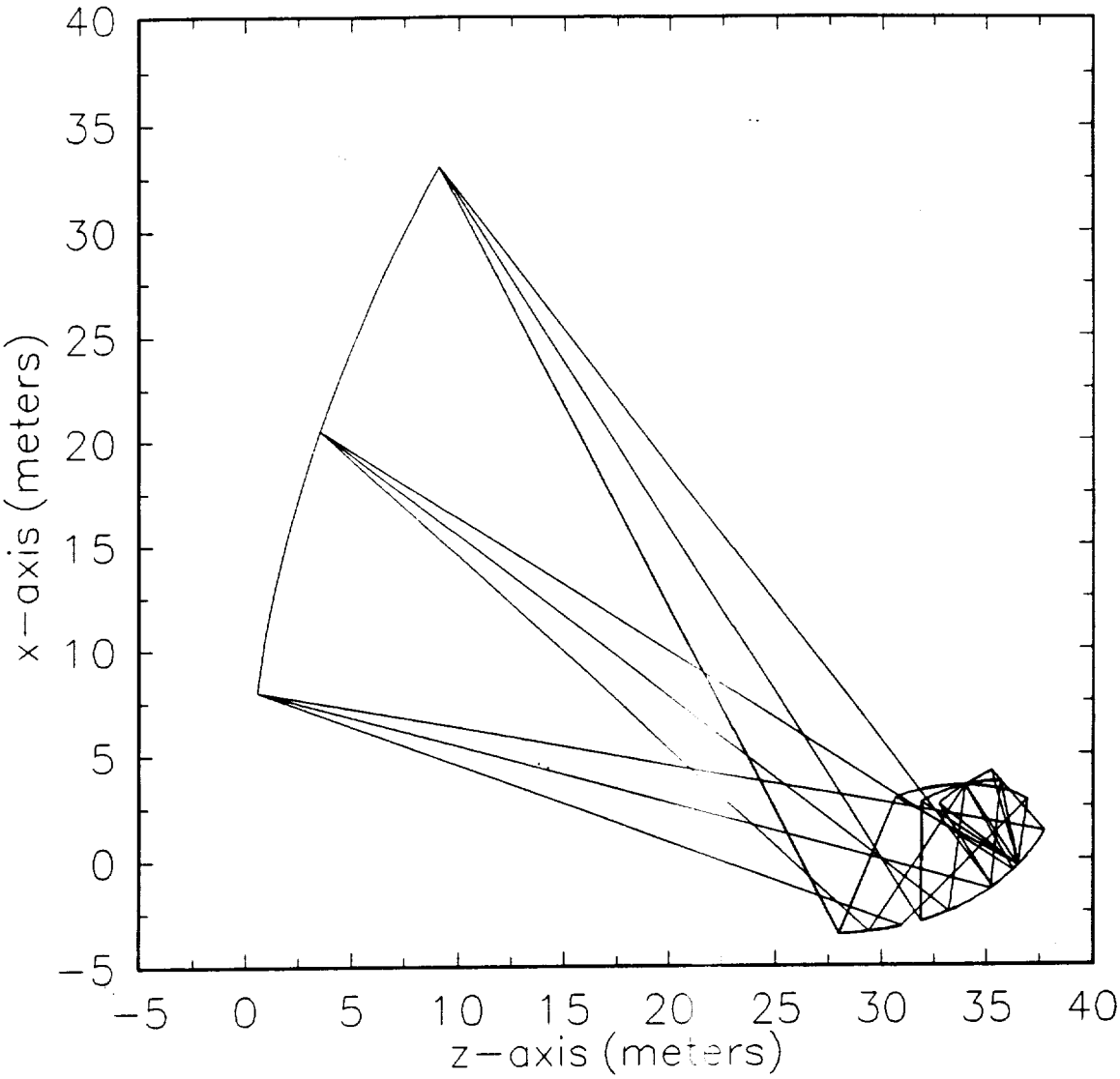

Figure 3-8. Gregorian tri-reflector antenna consisting of a parabolic main reflector, an elliptic subreflector in a Gregorian configuration and a shaped tertiary reflector. The feed is located on the subreflector (z = 36.5) which minimizes the scan induced phase error for the 5° scan direction. Shown is a system designed to scan ±5°.

[2] P. Foldes, "Characteristics of a Multireflector Antenna for High Resolution Radiometer with Large Angle Scan," Prepared for NASA Langley Research Center, Hampton, VA 23665-5225, contract NAS1-17209.

[3] W.L. Stutzman, K. Takamizawa, P. Werntz, J. LaPean, R. Barts, "Feasibility Study of a Synthesis Procedure for Array Feeds to Improve Radiation Performance of Large Distorted Reflector Antennas," Semiannual Status Report, Grant No. NAG-1-859, February 1991.

4. TYPE 6 REFLECTOR ANTENNA

The Foldes Type 6 antenna concept is discussed in this section and the dimensions are given. The optimization procedures used for the two and three dimensional synthesis are discussed. Results of MRAPCA (2D) and GRASP7 (3D) electromagnetic analysis of the scanning systems are shown.

4.1 The Type 6 Concept

The Foldes Type 6 concept is an offset Cassegrain dual reflector antenna with a limited scanning capability. Scanning over approximately a 1° total scan range is achieved with a fixed feed and small moving subreflector. The Cassegrain design of the Type 6 antenna allows a greater effective electrical focal length for a given mechanical size and minimizes aperture blockage. The overall dimensions of the Type 6 antenna are shown in Figure 4-1. A three dimensional view of the Type 6 concept is shown in Figure 4-2 (a-c).

4.2 Dual Reflector Antenna Synthesis (DRAS) Coding Approach

The synthesis of the Type 6 antenna is performed by the Dual Reflector Antenna Synthesis program. DRAS designs a correcting subreflector for a given scan angle and total path length (aperture plane to feed) and positions the available subreflector to minimize the error function between the unscanned and the correcting subreflector. The total path length is also optimized to find the correcting subreflector which best fits the available subreflector for each scan angle. The set of subreflector positions for each scan angle then determines the optimal scan path.

The error function between the correcting and the available subreflectors is

$$E = \sum_{i=1}^{N} \left[(\vec{S}'_i - \vec{S}_i) \cdot \hat{n}_{si} \right]^2 \qquad (4\text{-}1)$$

where S'_i is the available subreflector point, S_i is the correcting

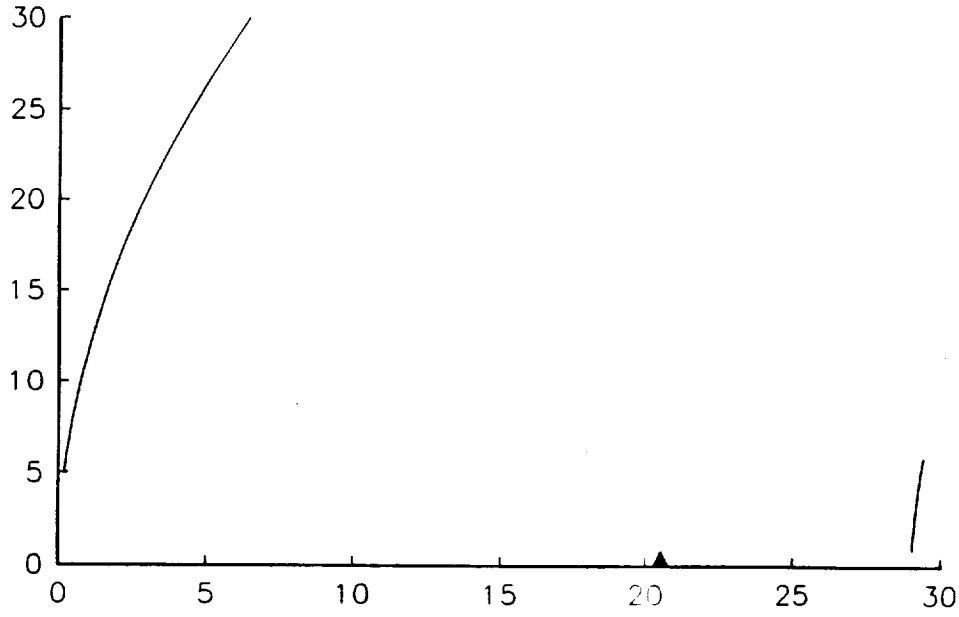

Figure 4-1. Type 6 Reflector Antenna System (profile view).

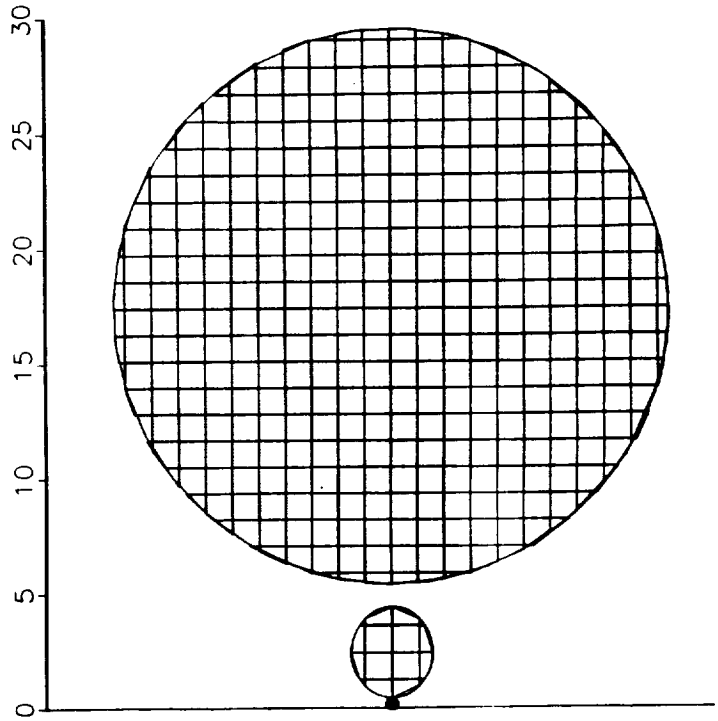

Figure 4-2a. Type 6 Reflector Antenna System (front view).

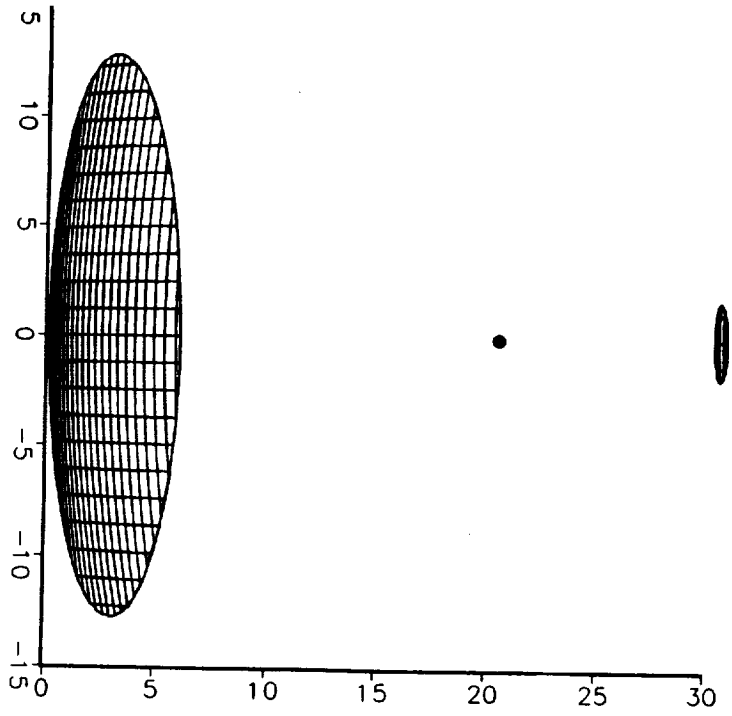

Figure 4-2b. Type 6 Reflector Antenna System (top view).

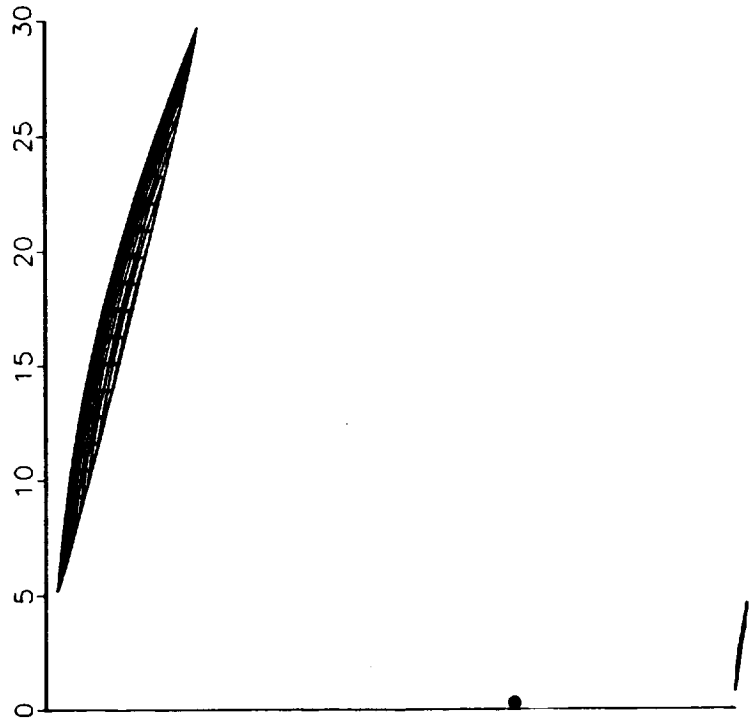

Figure 4-2c. Type 6 Reflector Antenna System (side view).

subreflector point, and n_{si} is the normal of the correcting subreflector at point i. In the three dimensional case, the summation is replaced with a double summation over the grid points of the subreflectors. This error function is proposed and found to give good results by Kitsuregawa [1].

4.3 Two Dimensional (Infinite Parabolic Cylinder) Synthesis Results

The initial electromagnetic analysis of the Type 6 system was performed for a two dimensional case to verify the synthesis approach. This analysis was performed with MRAPCA at 10 GHz with a main reflector diameter of ~28 meters and a focal length of ~35 meters. A single $\cos^q(\theta)$ feed was used and set to provide a 10 dB edge taper. This geometry resulted in an unscanned half-power beamwidth of 0.07° and -20 dB first sidelobes. Analysis of scanned systems indicated that the system would be capable of scanning over a total range of between 1.5 and 2.0 degrees. Figure 4-3 shows the results of this analysis for an unscanned system. Figure 4-4 and 4-5 show the results for systems scanned 0.5° down and 1.0° up, respectively.

4.4 Three Dimensional Synthesis Results

Analysis of the three dimensional Type 6 system is being performed with the TICRA GRASP7 reflector antenna package. Currently, analysis is at 10 GHz with a main reflector diameter of 25 meters and a focal length of 30 meters. A single feed with a Gaussian beam is used and provides an edge taper of ~15 dB. The unscanned system has a half-power beamwidth of 0.08° and first sidelobes of -28 dB. Figure 4-6 shows the analysis results for an unscanned system. Figures 4-7 through 4-10 show the results for systems scanned 1.0° and 0.5° down and up. These analyses were performed using the feed position, tilt, and beamwidth of the unscanned case. Analyses performed with feeds adjusted for each scan position show no appreciable improvement.

Absolute gain is calculated by GRASP7 and can be used as a figure of merit. A good definition of the scan range of the system is the range of scan with less than a one decibel gain loss. This definition results in a scan range of 1.0° for the Type 6 system at 10 GHz. The reduced scanning capability compared to the two dimensional case results from the more stringent definition of scan range. Sidelobe levels, the criteria for scan range in the two dimensional case, remain around -15 dB for scanning for up to ±1.0°.

4.5 Future Work

Future work with the Type 6 system will include the following:

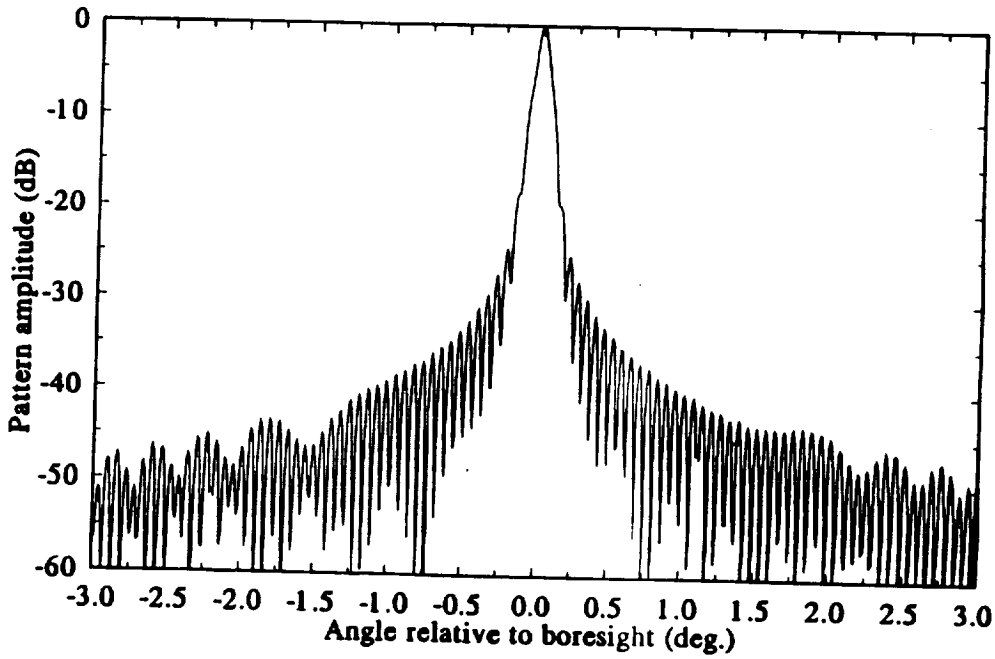

Figure 4-3. Type 6 Reflector Antenna System. Two dimensional analysis results (unscanned system).

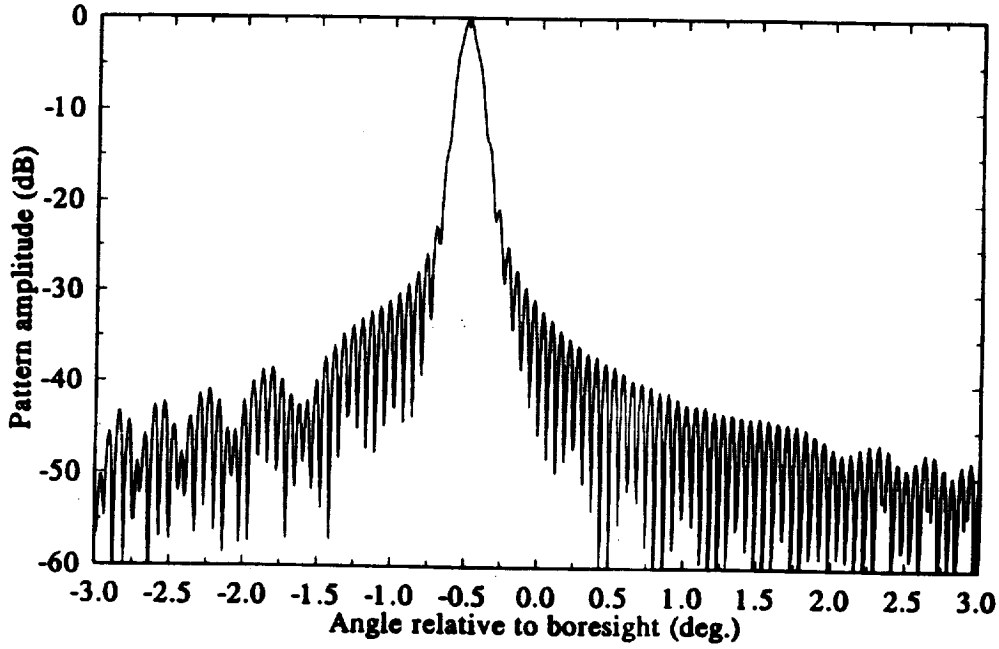

Figure 4-4. Type 6 Reflector Antenna System. Two dimensional analysis results (scanned 0.5° up).

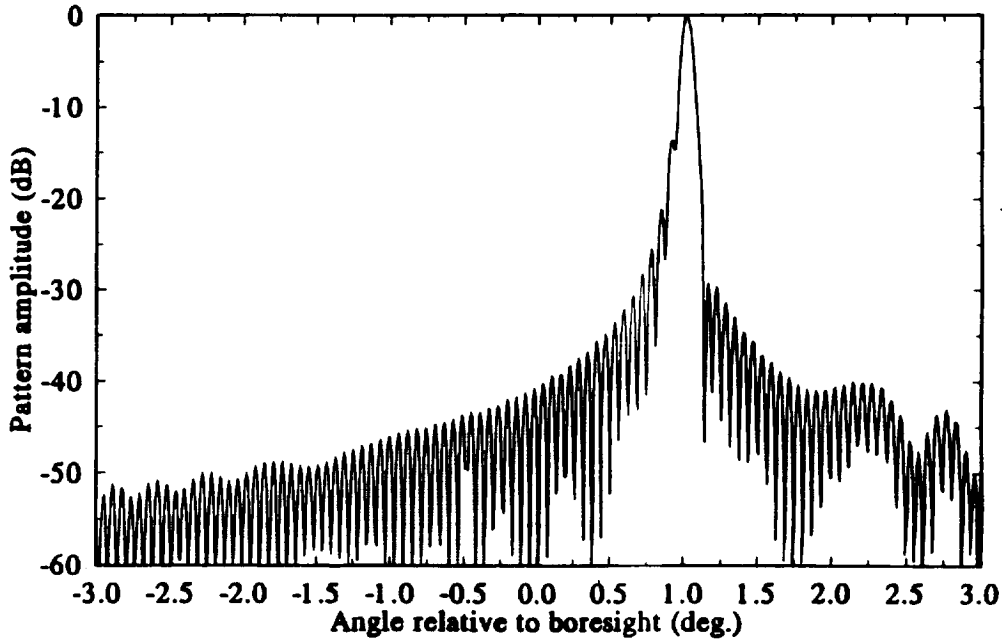

Figure 4-5. Type 6 Reflector Antenna System. Two dimensional analysis results (scanned 1.5° down).

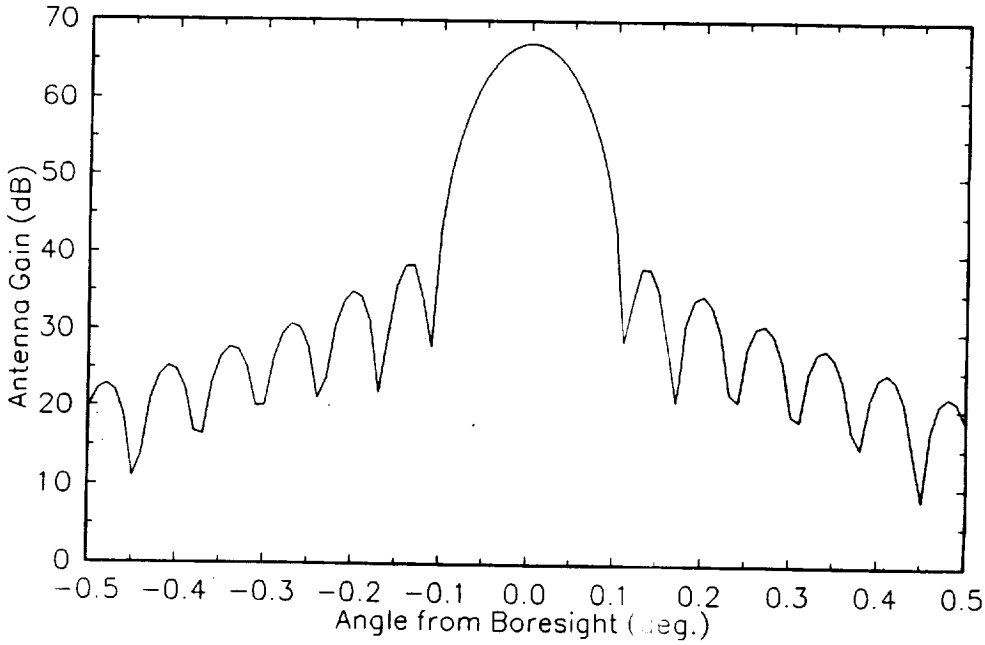

Figure 4-6. **Type 6 Reflector Antenna System. Three dimensional analysis results (unscanned system).**

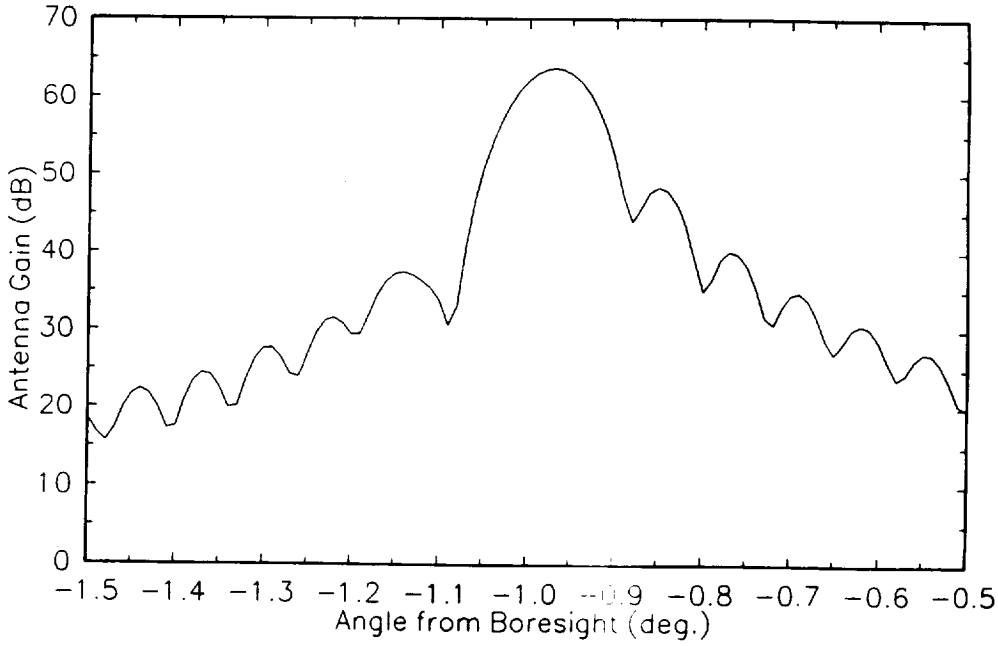

Figure 4-7. **Type 6 Reflector Antenna System. Three dimensional analysis results (scanned 1.0° down).**

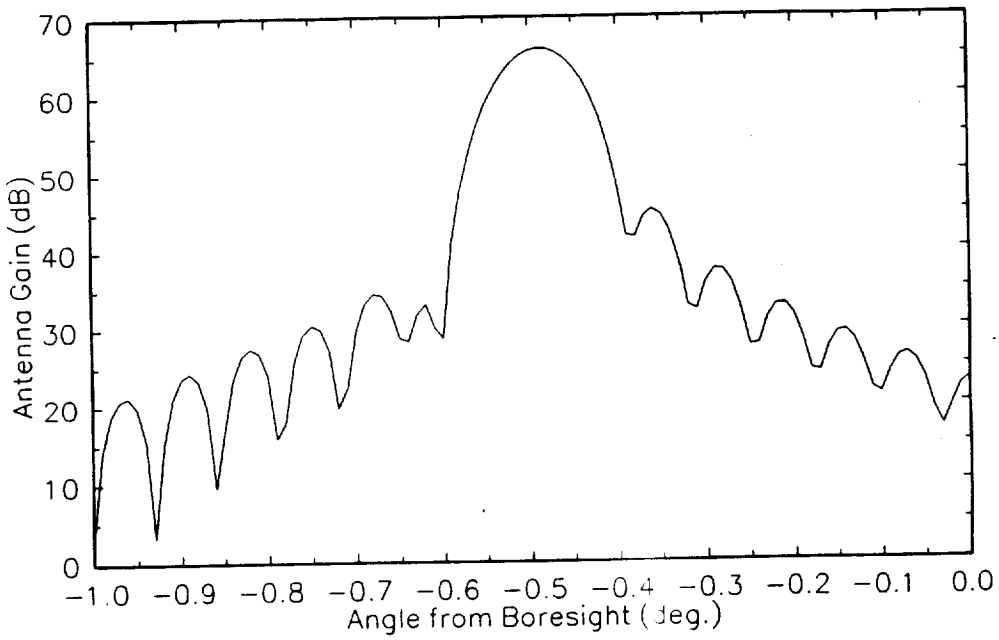

Figure 4-8. Type 6 Reflector Antenna System. Three dimensional analysis results (scanned 0.5° down).

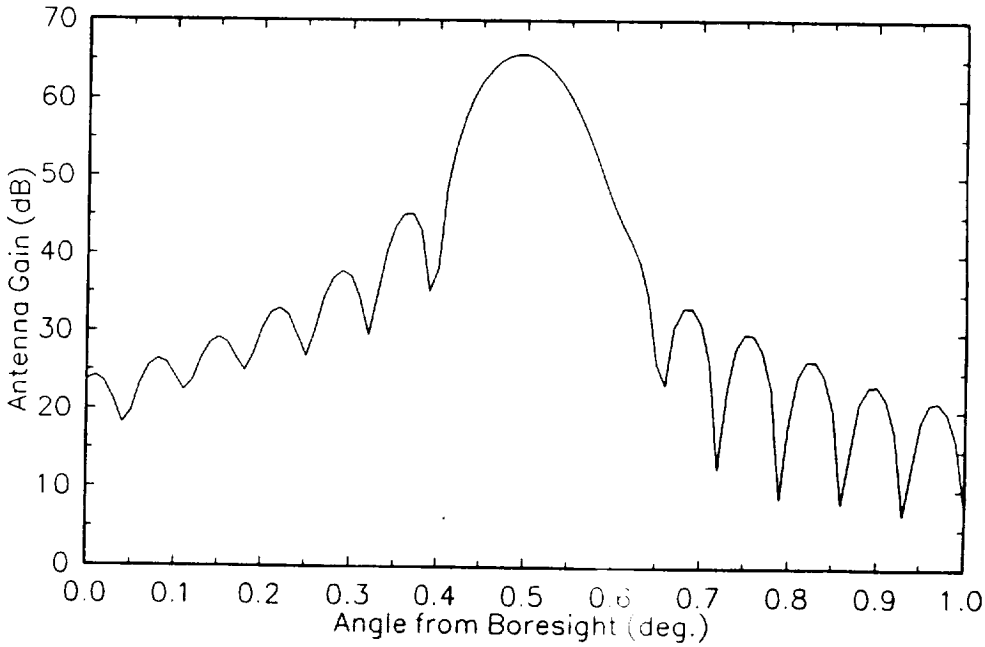

Figure 4-9. Type 6 Reflector Antenna System. Three dimensional analysis results (scanned 0.5° up).

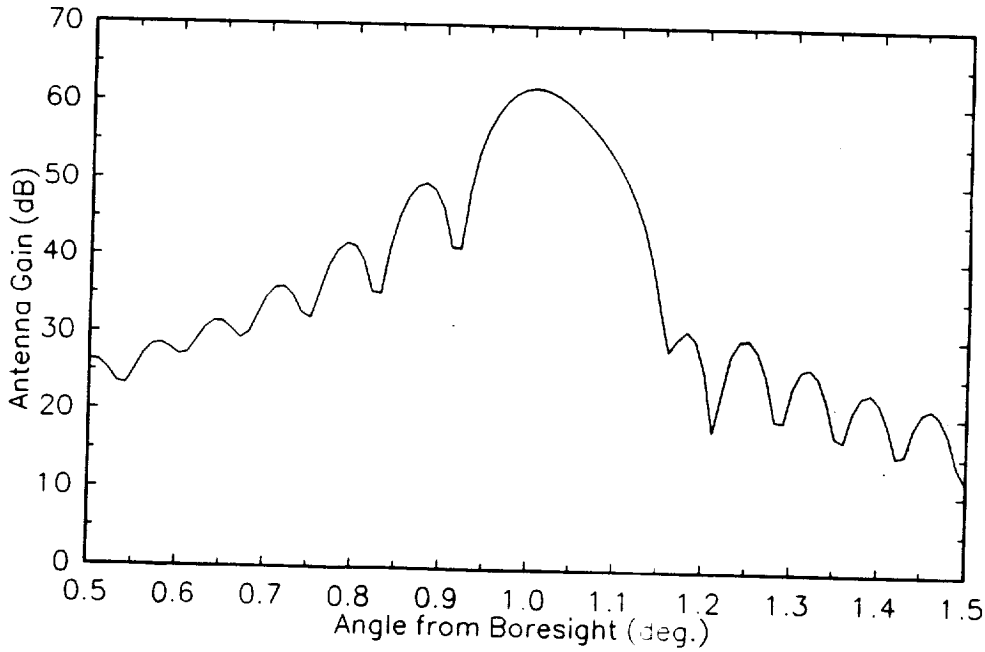

Figure 4-10. **Type 6 Reflector Antenna System. Three dimensional analysis results (scanned 1.0° up).**

(1) Completion of DRAS (3D) to allow scanning out of the plane of offset.

(2) Improvement of the subreflector error function.

(3) Analysis of the three dimensional Type 6 system at frequencies of 20, 40, and 60 GHz.

(4) Investigation of the possibility of scan improvement through the use of array feeds and the M.C. Bailey/Bill Smith sidelobe suppression techniques.

(5) Investigation of the possibility of scan improvement through the use of a dual shaped antenna system.

(6) Support for the electromagnetic testing of the NASA Langley AMRB/Space Structures Type 6 test article.

4.6 Suggestions for the NASA Langley Type 6 Test Article

Near-field electromagnetic testing of the Type 6 test article would be desirable to verify the synthesis and analysis approaches used to design the antenna system. The simplest test procedure would entail the construction of one or more subreflector surfaces to simulate scanned Type 6 systems. These surfaces could be repositioned by hand between tests and would provide a verification of the synthesis and analysis approach for the basic Type 6 system. A possible next step would be the development and installation of actuators to actively position the subreflector surface under test as would be done in a deployed system. An array-fed system using the M.C. Bailey/Bill Smith enhancement techniques could also be tested in either of these scenarios. Alternatively, an actively reshaped subreflector surface could be constructed to investigate the utility of active surface systems. Finally, a test of the complete system with a radiometric feed system could assist the development of the necessary radiometry techniques and data manipulation. This test could be achieved through a simplified sky survey using the Type 6 test article with the required radiometric support.

4.7 References

[1] T. Kitsuregawa, *Advanced Technology in Satellite Communications Antennas,* "Section 2.6 - Steerable Beam Antennas", pp. 177-178, Artech House, Boston, 1990.

5. GEOMETRICAL OPTICS SYNTHESIS FOR WIDE SCAN

The spherical reflector has an inherent spherical aberration which degrades the performance compared to a parabolic reflector. However, it scans without further degradation due to its spherical

symmetry. Scan is accomplished by mechanical movement of the feed. If a subreflector and tertiary reflector are added, the aberration can be corrected and the amplitude controlled. Then the whole feed assembly can be moved as a unit. The advantage is aberration-free scan; the disadvantage is movement of a large structure is required. Our initial results for the spherical tri-reflector antenna indicate that for an axially in symmetric system the GO aperture efficiency can be as high as 70% and as high as 50% for the offset configuration. These are for a uniform amplitude distribution over the illuminated portion of the main reflector and ± 5° scan.

A related effort is a GO synthesis technique using the SORT (Scan Optimization Ray Tracer) code. Here all reflector shapes are variables. Multiple subreflectors are used to reduce the image region. Then a single feed (or small feed array) is moved over the image region, which is much smaller than that used for the previous spherical reflector.

6. OPTIMIZATION OF REFLECTOR CONFIGURATIONS USING PHYSICAL OPTICS

The geometrical optics (GO) is, by far, the most widely accepted technique used for the design of reflector antennas. GO is a high frequency approximation to the electromagnetic fields which employs rays to describe the fields incident from the source and the fields reflected and refracted at an interface between two media. In the GO based synthesis of reflector antenna systems, the geometry of some or all of the reflectors and/or location and radiation patterns of the feed elements are determined by solving equations derived from the rays between the feed location and the aperture plane of the reflector systems.

The GO based techniques have been shown to work well in many cases. Both Type 2 and Type 6 configurations described in Chapter 3 and 4 are synthesized based on GO techniques. The GO synthesis, however, cannot include detailed specifications on the performance parameters such as the cross-polarization components, the far-outside sidelobe envelopes, the null positions and the beam efficiencies. When these parameters are specified, the GO techniques usually require "fine tuning" of the reflector geometry by repeated application of post synthesis radiation pattern analysis using physical optics (PO) and diffraction techniques.

An alternative method to synthesize reflector antenna is to use physical optics. The technique allows to specify the performance parameters in the synthesis process. Unfortunately, it is not possible to solve for reflector configurations directory from the physical optics for a given feed pattern and a desired radiation pattern because it is not possible to invert the PO surface integral for an arbitrary reflector geometry. A technique to solve for the reflector configuration is to convert the problem

to that of minimization. A functional which represents the differences between desired and calculated performance parameters can be defined and it can be minimized using an iterative technique.

Physical Optics Optimization Program (POOP) is a computer program implementing the physical optics synthesis technique in 2-dimension. POOP uses routines from the analysis program, MRAPCA [See Section 2.1], to compute the aperture fields or far fields of the reflector systems. Powell's method is used to minimize the functional which is defined as the sum of RMS differences in the desired and the calculated aperture fields of main reflector in M-scan directions.

As an example, application of POOP to the Gregorian Type 2 reflector configuration discussed in the previous semiannual status report [Feb. 1991, Section 3.2] is considered (main reflector with D=30 m, F=40 m). In particular, the reflector configuration designed for 0° scan is slightly modified to optimize the radiation pattern for -5° scan at 1 GHz. Two cases are considered: 1) the location and the orientation of tertiary reflector and the orientation of the feed are allowed to change, 2) in addition to the variables in case 1 the subreflector shape is also allowed to change.

Figure 6-1 shows the amplitude and phase distributions of aperture fields for the desired and the unoptimized configurations. The fields for the unoptimized reflector are calculated using the tertiary reflector for 0° scan, with 11.2° rotation and zero translation to scan the main beam to -5°. The large discrepancy between the desired and the unoptimized fields causes higher sidelobe level, gain reduction, and main beam pointing error.

Figure 6-2 and 6-3 show the resulting aperture field distributions for cases 1 and 2, and Table 6-1 shows a summary on the required movement of the tertiary reflector. Considerable improvements in the aperture fields for both cases can be observed. In particular, Fig. 6-2 shows that majority of aperture fields error can be corrected by slight movement of the tertiary reflector (0.43 meter translation and 0.5° rotation from unoptimized tertiary reflector). It can be also concluded from Fig. 6-3 and Table 6-1 that the required transnational movement of the tertiary reflector can be significantly reduced by shaping the subreflector.

Figs. 6-2 and 6-3 show that aperture fields can be improved by PO optimization, however, it is difficult to compare the quality of the aperture fields between case 1 and case 2 from the figures. One of ways to quantify the quality of aperture fields is to look at the Sidel aberration coefficients of the aperture phase distribution. The aberration coefficients are determined by expanding the aperture phase distribution $\phi(\chi)$ in power series

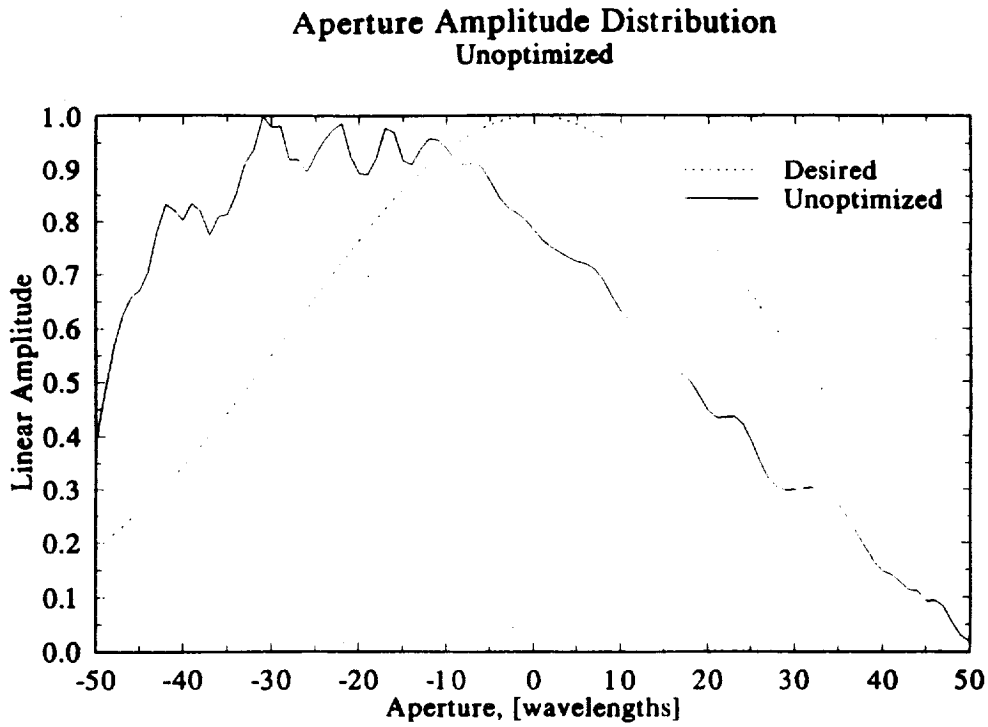

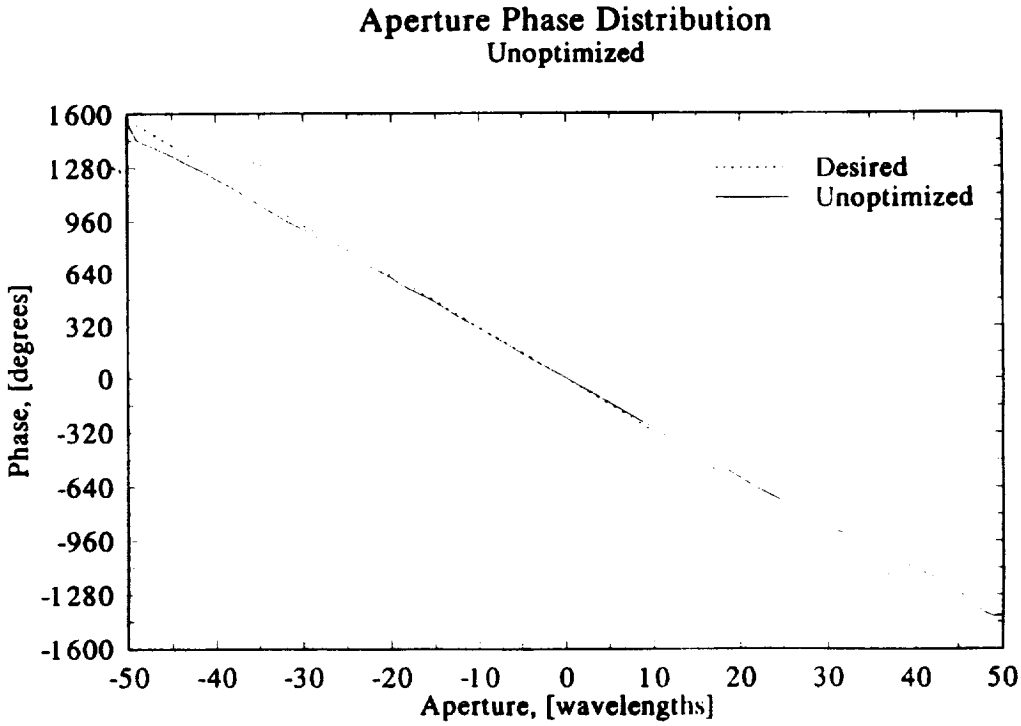

Figure 6-1. The aperture field distributions for the desired and the unoptimized reflectors. a) amplitude, b) phase.

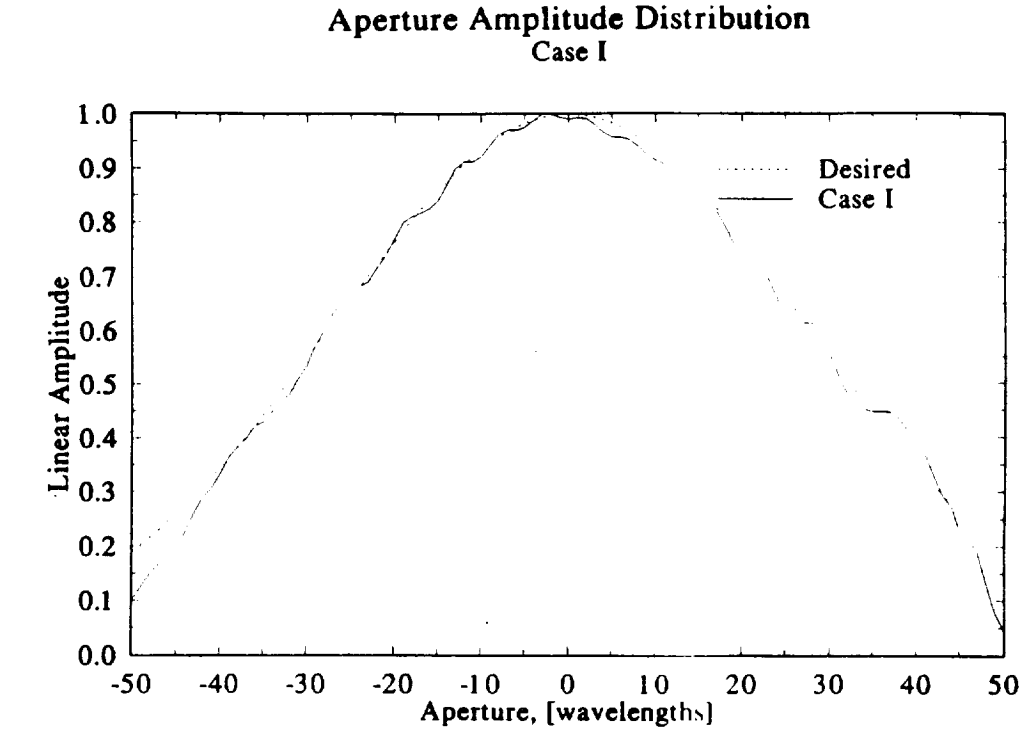

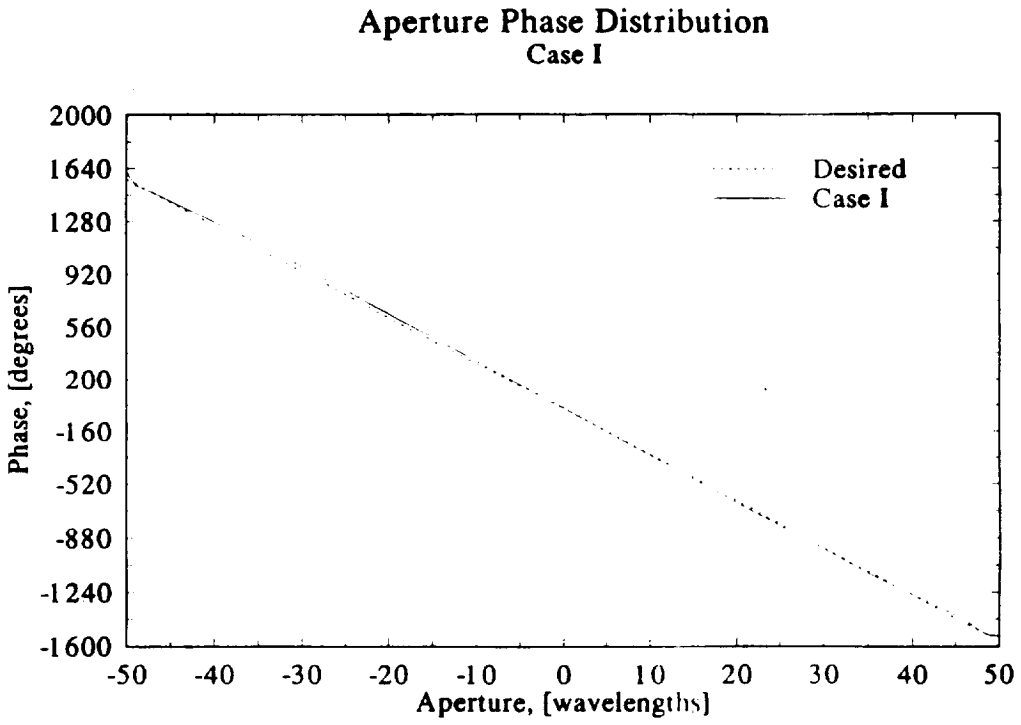

Figure 6-2. The aperture field distributions for the desired and the case 1 optimized reflectors. a) amplitude, b) phase.

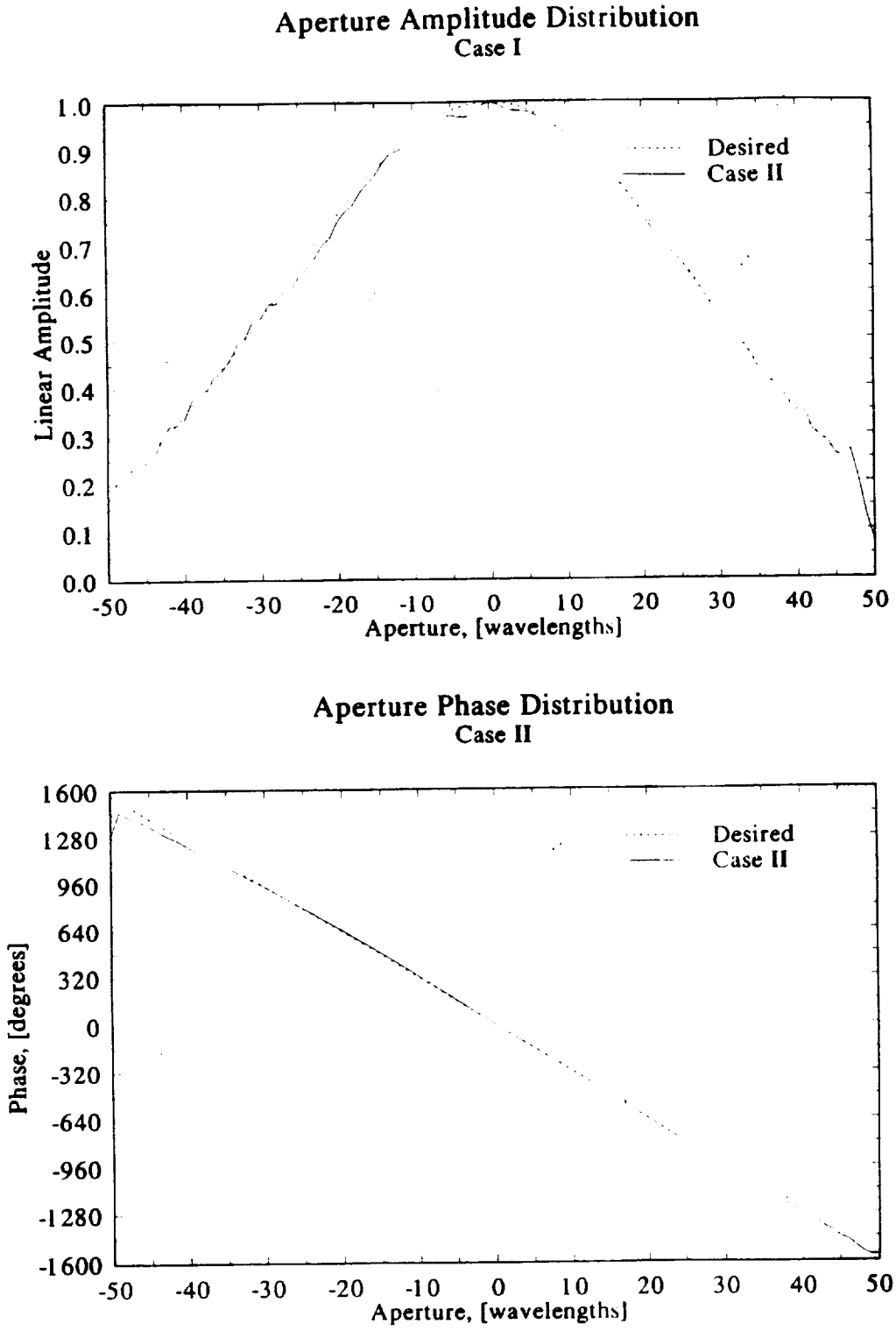

Figure 6-3. The aperture field distributions for the desired and the case 2 optimized reflectors. a) amplitude, b) phase.

$$\phi(\chi) = \alpha_0 + \alpha_1\chi + \alpha_2\chi^2 + \alpha_3\chi^3 + \alpha_4\chi^4 + \ldots$$

where χ represents a location in aperture in wavelength. The coefficients are classified in terms of types of aberration as

α_0 = offset
α_1 = linear error
α_2 = quadratic error
α_3 = comma error
α_4 = spherical error

The first two coefficients α_0 and α_1 are not part of the aperture phase error. α_0 corresponds to the phase offset relative to the phase reference. α_1 is the phase tilt in the aperture which scans the main beam to the desired location. The higher order aberration coefficients, α_i $i \geq 2$, cause degradation in the secondary pattern.

Table 6-2 shows the aberration coefficients of aperture phase distributions for unoptimized and optimized configurations. It is apparent from the table that the optimization reduced the error in the linear phase error, α_1. The parabolic aberration, α_2, is also reduced for the case 2, where as it is increased slightly for the case 1. The comma aberration α_3, however, increased for both case 1 and case 2. The results suggests that the definition of error function must incorporate the Sidel coefficients to reduce the beam degradation due to aberration.

Table 6-1

Required tertiary reflector movement for the unoptimized and the optimized reflectors.

	X	Z	Total	Rotation
Unoptimized	0.00 m	0.00 m	0.00 m	11.2°
Case 1	0.30 m	0.31 m	0.43 m	11.7°
Case 2	0.03 m	0.12 m	0.13 m	11.5°

Table 6-2

Aperture field aberration coefficients for the unoptimized and optimized reflectors.

	α_1	α_2	α_3
Desired	-31.9	0.00×10^{0}	0.00×10^{0}
Unoptimized	-29.9	1.04×10^{-2}	6.05×10^{-4}
Case 1	-32.8	1.13×10^{-2}	7.05×10^{-4}
Case 2	-32.5	-1.05×10^{-3}	8.34×10^{-4}

Future work includes the following

(1) Continue the synthesis of the type-2 reflector system configuration in 2-dimension which are optimized for M-scan directions, and N-frequencies.

(2) An investigation into the definition of error functional based on the specifications on beam efficiency, aberration coefficients and scan loss, which can be used in the generalized aperture synthesis of reflector antennas.

(3) Extension of optimization technique to 3-dimension.

7. RADIOMETRIC ARRAY DESIGN

This project is reported on in detail in a separate annual report. Here we only highlight the progress of this effort.

In the development of the reflector concepts it is taken for granted that a small feed array will be needed for beam steering and surface distortion correction. This effort is aimed at developing array analysis and design techniques for radiometric applications.

We have developed a generalized analytical model to characterize the effects of noise contributions from the array feed based on the scattering parameters of each part of the array, feed network, and radiometer receiver.

Our model represents the array and feed network as multiport networks characterized by their scattering parameters. The scattering parameters of the array characterize the element mismatch and interelement mutual coupling. The feed network scattering parameters characterize the mismatch at each port of the network, the transfer function of the network and cross coupling between ports of the network.

Noise contributions are included in the model as noise voltage sources. The external noise environment impresses a received voltage on each element of the array. It is these noise voltages that are the desired quantity to be measured by the radiometer. Noise contributions due to the feed network are modeled as voltage sources at each port of an equivalent noiseless network. These sources can include noise due to both active and passive devices within the feed network. Figure 1 illustrates conceptually our model for an array and associated feed network. Using this same approach, the effects of receiver noise contributions are also included in the model.

From this conceptual model we have developed a network model based on the scattering parameters as described above. Mathematically the network can be described by three matrix

equations, one each for the array elements, the feed network, and the receiver. Using these matrix equations we have developed an expression for the total received voltage at the receiver. This expression includes the effects of all noise sources in the system; the external noise environment, contributions from the feed network, and contributions from the receiver. From this expression for the received voltage, the total received power, the actual measured quantity in a radiometric system, can be found. To our knowledge, no one has previously examined noise effects in an array in such a generalized manner.

In our model, the internal and external noise sources are assumed to be measurable or derivable quantities. The noise temperature of the ports of a passive linear multiport, such as a power divider/combiner that might be used for the feed network, can be directly calculated from the scattering parameters of the network and has been previously derived. Thus for any passive linear multiport, the noise model for the multiport is derivable from the multiport scattering parameters. Using a microwave CAD package for the analysis of device scattering parameters, we have been able to derive noise models for passive multiport devices such as Wilkinson hybrid power dividers.

Calculation of the received external noise sources is complicated by the fact that the noise voltage impressed on the array elements has a spatial variation that depends on the total scene being observed. The array feed noise model we have developed allows us to predict the effect of the network on received external noise but does not tell us how the external noise scene interacts with the array elements. Currently we have developed a rudimentary model for the external noise scene/array interaction and are investigating its accuracy and usefulness.

The received noise power model we have developed can be used to evaluate the relative merits of various array configurations and feed network architectures. One design issue of particular interest that we are pursuing is the use of active devices in the feed network, i.e. low noise amplifiers and electronically controlled phase shifters.

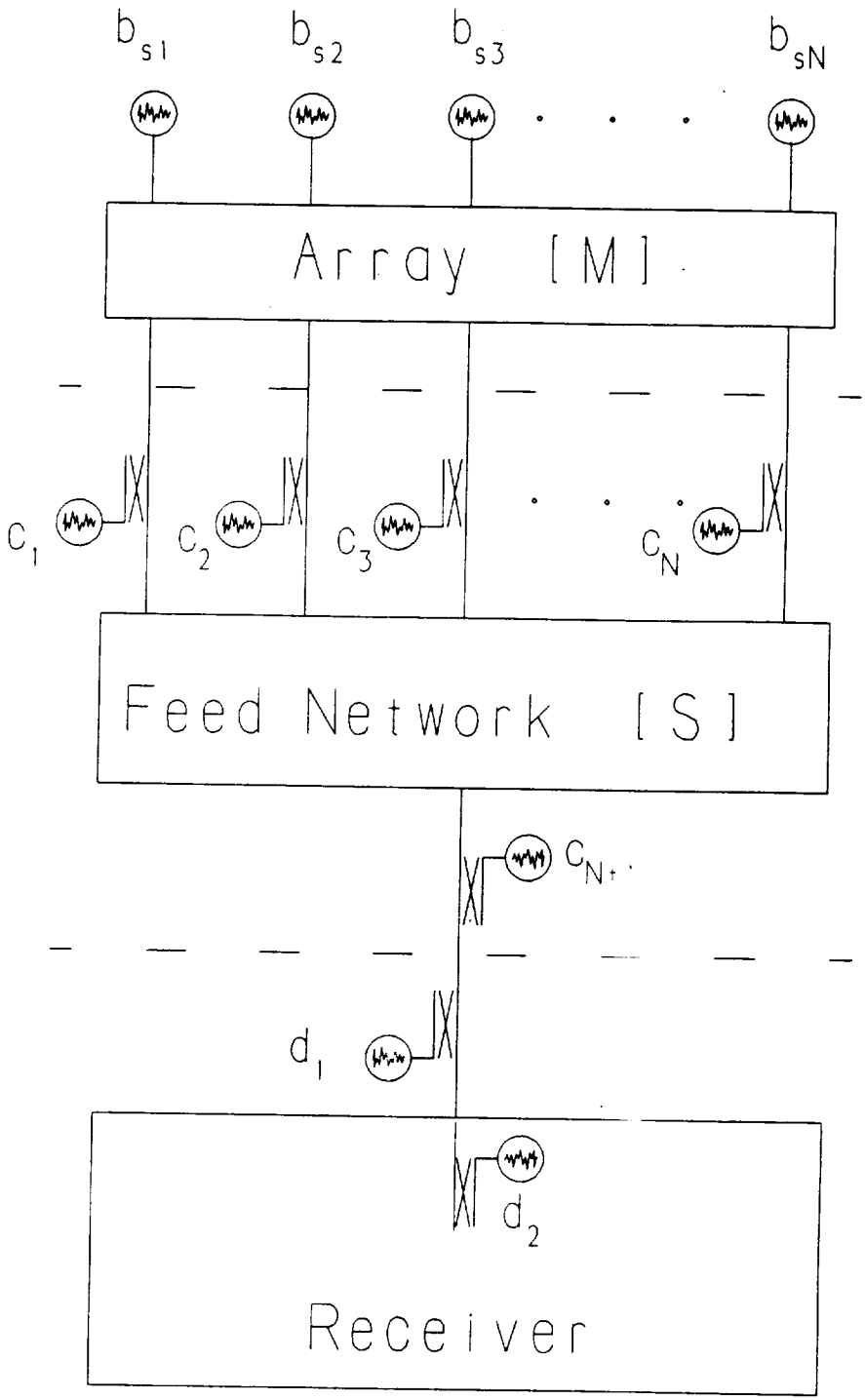

Figure 7-1. Array noise model.